DOI: 10.1002/ejic.200900199

Dielectric Constant Controlled Solvothermal Synthesis of a TiO_2 Photocatalyst with Tunable Crystallinity: A Strategy for Solvent Selection

Jianjun Wu,[a,b] Xujie Lü,[a] Linlin Zhang,[b] Fuqiang Huang,*[a] and Fangfang Xu*[b]

Keywords: Photocatalysis / Solvothermal synthesis / Crystal engineering / Titania / Oxo ligands

Phase-pure anatase TiO_2 nanocrystals with a tunable crystallinity have been prepared by a one-step solvothermal method in the absence of any templates or additives. The crystallinity can be successfully controlled by varying the dielectric constant of the reaction solvent. 2-Propanol, which has the lowest dielectric constant of those studied, favors the crystallization of TiO_2 nanocrystals with the best crystallinity, in other words nano-TiO_2 crystals with the largest crystallite size (14.8 nm), lowest lattice strain (7.27×10^{-3}), and highest photocatalytic efficiency (almost six times that obtained in methanol). The effect of the dielectric constant on the solubility of the precursor and subsequent nucleation and crystal growth is discussed in detail. These discussions shed some light on solvent selection for the designed synthesis of nano-TiO_2 with different crystallinity. The photocatalytic activity of the as-prepared samples has also been investigated with respect to their crystallinity.

Introduction

Semiconductor nanoparticles have been a subject of great interest due to their size-tunable physical and chemical properties and potential applications.[1] In light of its low-cost, wide availability, nontoxicity, and physicochemical stability, titanium dioxide (TiO_2) has attracted a great deal of attention during the past decade. TiO_2 is widely used in various areas because of its versatile properties,[2] such as catalytic activity,[2a] photocatalytic activity for pollutant removal,[2b] good stability toward adverse environments,[2c] dielectric character,[2d] photoelectrochemical conversion,[2e] sensitivity to humidity and gas,[2f] nonlinear optics,[2g] and photoluminescence.[2h] Photocatalysis has been extensively studied as a potential solution to the recent severe problems of energy shortages and environmental crises, especially since Fujishima and Honda announced a TiO_2-based photochemical electrode for splitting water in 1972.[2i]

Of the three polymorphic phases, the photocatalytic activity of metastable anatase TiO_2 with an appropriate crystallite size is higher than that of either rutile or brookite,[3] especially when decreasing the particle size to the nanometer scale. The catalytic activity at these scales is greatly enhanced, because the optical bandgap is widened due to the quantum size effect and due to the increased surface area.[4]

Various techniques[5] have been reported for the preparation of nano-TiO_2, such as solvothermal synthesis,[5a] hydrolysis-precipitation,[5b] sol-gel methods,[5c] chemical vapor deposition,[5d] and thermal decomposition of alkoxides.[5e] Although sol-gel methods are widely used to prepare nano-TiO_2, the precipitated powders are amorphous in nature, and the resulting post-calcination process required inevitably results in particle aggregation, a reduction in specic surface area, and even phase transformations. The solvothermal method[6] is an alternative route for direct (one-step) synthesis of pure anatase nano-TiO_2. However, most attention is usually directed toward control of the structure and morphology by varying the reaction temperature,[7] reaction time,[8] additives,[9] and pH[10] during solvothermal treatment, whereas another important experimental parameter, namely the solvent, has rarely[11] been varied with the aim of achieving different well-crystallized nanostructures.

Our understanding of, and ability to control and monitor, crystal nucleation and growth is still rudimentary even though these processes are of central importance to living systems and in pure and applied sciences. Initial failures to obtain the solvothermal growth of a specific compound are usually the result of a lack of data regarding the type of solvent, the solubility, and solvent–solute interactions.[12] Solubility is a vital physicochemical and technological parameter which strongly influences the rate of dissolution and degree of supersaturation, and therefore the rate of nuclei formation.[13] Solubility depends upon the nature of the substance, its aggregation state, temperature, pressure, and a series of other factors, among which the dielectric con-

[a] CAS Key Laboratory of Materials for Energy Conversion, Shanghai Institute of Ceramics, Chinese Academy of Sciences (SICCAS),
1295 DingXi Road, Shanghai 200050, P. R. China
Fax: +86-21-52416360
E-mail: huangfq@mail.sic.ac.cn
[b] Inorganic Materials Analysis and Testing Center, SICCAS, Shanghai 200050, P. R. China
E-mail: ffxu@mail.sic.ac.cn

Supporting information for this article is available on the WWW under http://dx.doi.org/10.1002/ejic.200900199.

stant has a crucial effect on precursor solubility due to the diverse solvation energy. However, this field has rarely been explored in the literature, to the best of our knowledge, especially for the solvothermal synthesis of nano-TiO_2. We have therefore studied the formation of well-crystallized TiO_2 nanoparticles by a one-pot solvothermal route. The effect of the dielectric constant on the solubility of the precursor and subsequent nucleation and crystal growth is discussed herein in detail with the aim of shedding some light on the process of solvent selection for the designed synthesis of nano-TiO_2. Moreover, the photocatalytic activity of the samples has also been fully investigated in light of their crystallinity.

Results and Discussion

Phase and Morphology of the Nanoparticles

Figure 1 shows the XRD patterns for the powders synthesized in four different alcohols. Hereafter, Et-240 (or -180) will be used to denote nano-TiO_2 treated at 240 °C (or 180 °C) for 6 h with ethanol as solvent (Me, Pr and Bu indicate methanol, 2-propanol, and *n*-butanol, respectively). All the powders except for Me-180 belong to the anatase type of TiO_2 (JCPDS 21-1272), with no contamination from other crystalline phases. The lack of diffraction peaks in the spectrum for Me-180 indicates that this sample is composed of amorphous particles, and crystallization only occurs above 180 °C, as confirmed by the XRD pattern for Me-240 shown in Figure 1b. Pr-180 and Pr-240 (reaction temperatures of 180 and 240 °C, respectively) show the sharpest peaks, thus indicating the relatively high crystallinity of these two samples.[14] This aspect will be discussed further below.

A typical UV/Vis spectrum for the obtained nano-TiO_2 samples is shown in Figure 2. To obtain more precise optical bandgaps, $(\alpha h\nu)^{1/2}$ was plotted against the absorption energy of Pr-180 because of its indirect transition nature.[15] E_g was found to be 3.09 eV, which falls in the range reported previously.[16] Furthermore, this value of E_g enables the powder to have a sufficient absorption in the ultraviolet range (< 400 nm), which is of importance for a UV light driven photocatalyst.

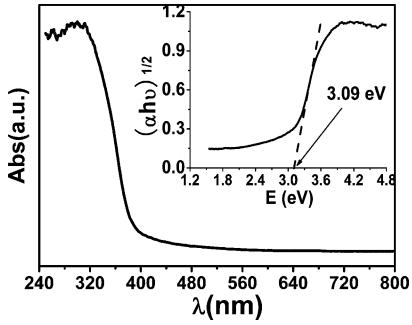

Figure 2. UV/Vis spectrum for a typical nano-TiO_2 sample.

The TEM images for samples obtained at 240 °C are presented in Figure 3, where it can clearly be seen that the crystallite size and shape strongly depend on the type of the solvent employed. Thus, particles with an amorphous shape are severely agglomerated and poorly crystalline when synthesized in methanol (Me-180, shown in the Supporting Information), whereas the crystallinity of Pr-240 is significantly enhanced and the particles tend to exhibit an equiaxed geometry bounded by crystallographic facets. The HRTEM image confirms the anatase structure for Pr-240. The inset shows the lattice image of a TiO_2 particle and its FFT diffractogram, which is consistent with a [100]-projected diffraction pattern of anatase-type TiO_2. Among all the four powders obtained at 240 °C, Pr-240 (S_{BET} = 88.2 $m^2 g^{-1}$) has the largest crystallite size (about 15 nm), as determined from the corresponding TEM image. As the samples described herein were synthesized under the same conditions of temperature and time, their different morphologies and XRD patterns should originate from use of different solvents.

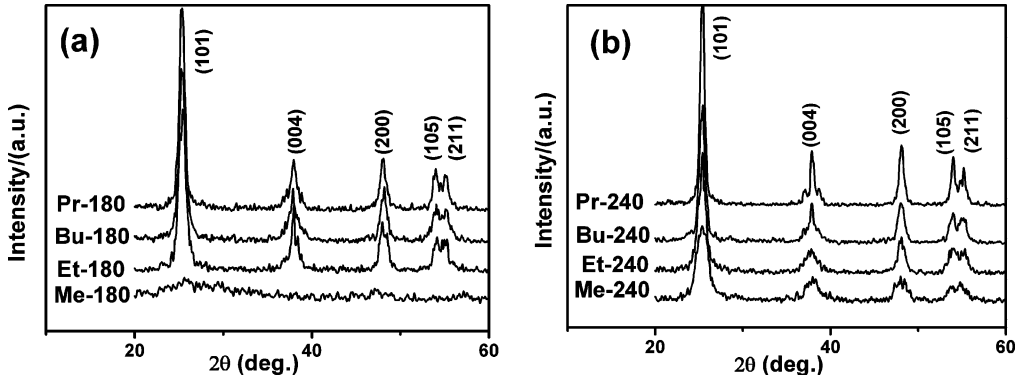

Figure 1. XRD patterns for samples obtained at (a) 180 °C and (b) 240 °C.

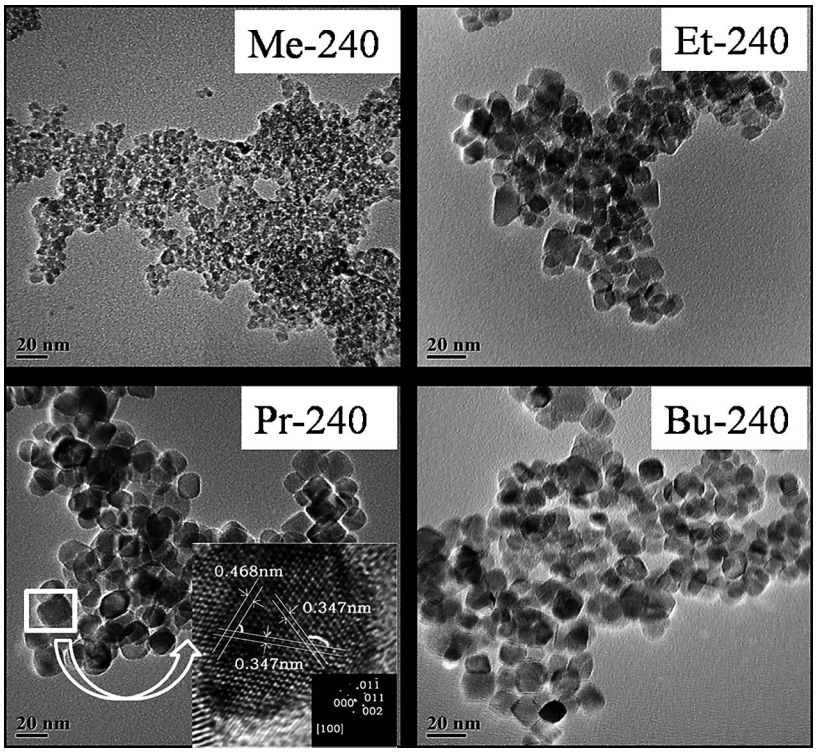

Figure 3. TEM images for the TiO_2 nanoparticles obtained at 240 °C.

Photocatalytic Performance of the Nano-TiO_2

Figure 4 depicts the result of the photocatalytic degradation of methyl orange (MO) in the presence of nano-TiO_2 samples. The photocatalytic efficiency decreases gradually in the order Pr-240 > Bu-240 > Et-240 > Me-240, in agreement with the decreasing crystallite size (see Figure 4b). A similar situation was found for the samples synthesized at 180 °C (Figure 4a). Pr-240 showed the highest photocatalytic efficiency, degrading more than 92% of the MO in 40 min, whereas Me-240 photodegraded less than 36% of MO in 40 min under the same conditions. A quantitative discussion of the reaction kinetics for this reaction and the dependence of the photocatalytic activity on the crystallinity can be found below.

The Effect of the Dielectric Constant on the Crystallization

Crystallite size (D) and lattice strain (ε) were calculated by using the Williams and Hall equation[17] (see Experimental Section); plots of $\beta\cos\theta$ vs. $\sin\theta$ based on the XRD patterns (Figure 1b) are shown in Figure 5. These plots show relatively good linearity for Et-240, Bu-240, and Pr-240, which allows us to determine reliable values for D and ε. For poorly crystalline samples such as Me-240, however, the number of diffraction lines detected was limited as some of them are so weak and broad that β is difficult to measure, therefore the experimental points for the diffraction lines measured are scattered.[14,18] The accuracy of the D and ε values is therefore not so high. Table 1 lists the quantitative values of D and ε for each sample. The calculated D values

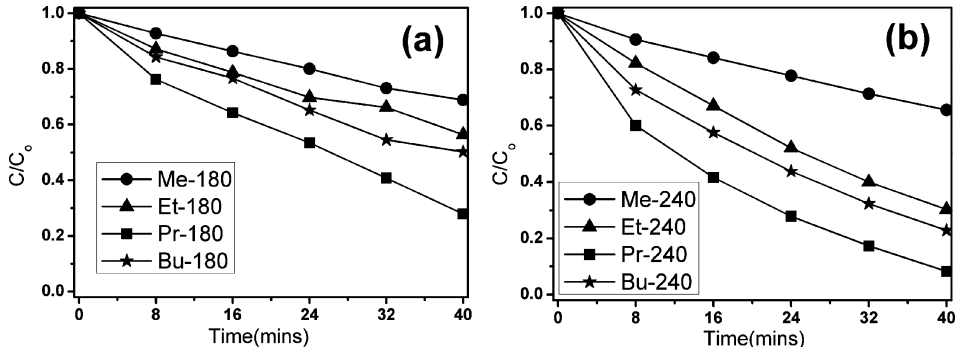

Figure 4. Photodegradation of MO over samples under UV irradiation.

display a good agreement with the data determined from the TEM images, with crystallinity increasing, in other words crystallite size increasing and lattice strain decreasing, in the order Me-240 < Et-240 < Bu-240 < Pr-240, thereby indicating that the crystallinity of the nano-TiO_2 samples is strongly dependent on the solvent used.

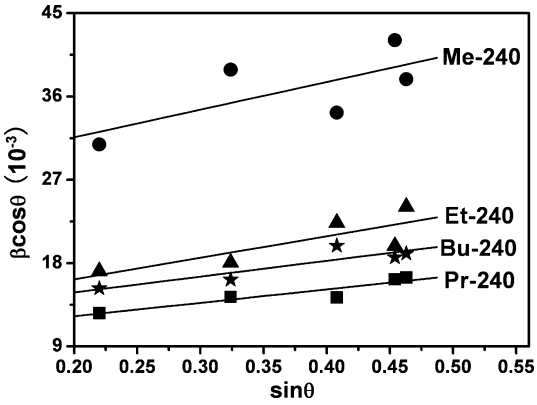

Figure 5. The relation between $\beta\cos\theta$ and $\sin\theta$ for the samples obtained at 240 °C.

Table 1. D and ε values obtained from the data shown in Figure 5.

	D [nm]	ε (10^{-3})
Me-240	5.7	14.94
Et-240	11.6	11.87
Bu-240	12.2	8.56
Pr-240	14.8	7.27

Solvents with different physicochemical properties have a pronounced effect on the crystallinity and morphology of the final nanocrystals by influencing the solubility, reactivity, diffusion behavior, and crystallization kinetics (crystal nucleation and growth rate).[19] Although great importance[20] has been attached to solvent polarity, coordinating ability, saturated vapor pressure, viscosity, and steric hindrance in the various syntheses reported in the literature, the effect of the dielectric constant has rarely been discussed. Here, we provide a closer look at the effect of the dielectric constant on the crystallinity of the nano-TiO_2 samples obtained.

The crystallization of nanoparticles generally consists of two processes:[21] nucleation and crystal growth. The nucleation rate, J_N, can be expressed as follows with a pre-factor, J_0:[13]

$$J_N = J_0 \exp\left(\frac{-16\pi V_m^2 \gamma^3}{3(RT)^3(\ln S)^2}\right)$$

$$S = C_l / C_s$$

where V_m is the molar volume of the solid material, S is the supersaturation degree, C_l the precursor concentration, C_s the solubility of the solid phase, J_0 the frequency of collisions between precursor molecules, γ the interfacial tension, R the gas constant, and T the temperature. Hence, it can be concluded that the nucleation rate is expected to increase strongly with increasing supersaturation. The solubility of an inorganic salt decreases with a decrease in the dielectric constant of the solvent due to the decreased solvation energy.[22] During the crystal growth process, larger particles grow at the expense of smaller ones due to the energy difference between the larger particles and the smaller ones with higher solubility based on the Gibbs–Thompson law. This so-called "Ostwald ripening" process has been applied and confirmed in numerous papers.[19a,23] In methanol, as can be seen from Table 2,[24] a higher dielectric constant (η = 32.35) results in a higher solubility of the solid metal oxide and a lower supersaturation degree in this system, which leads to fewer nuclei, a reduced precursor supply rate, and slower crystal growth,[12,19,20d] and therefore lower crystallinity (see Figure 6). As mentioned above, the crystallinity (crystallite size and lattice strain) of the obtained nano-TiO_2 should follow the order: Me-240 < Et-240 < Pr-240 < Bu-240. However, the present data show some unexpected results, namely that Pr-240 has better crystallinity than Bu-240, thus showing that other solvent properties, such as viscosity, saturated vapor pressure, coordinating ability, and steric hindrance, should be taken into account.[20] In other words, crystallinity depends on the dielectric constant of the solvent to a large extent, but not exclusively.

Table 2. Dielectric constant for the alcohols used.

	Methanol	Ethanol	2-Propanol	*n*-Butanol
Dielectric constant[a]	32.35	25.00	18.62	17.50

[a] Data taken from ref.[24]

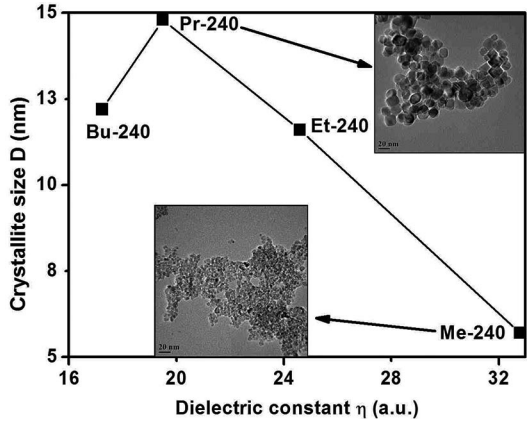

Figure 6. The effect of the dielectric constant on the crystallinity.

The Dependency of the Photocatalysis on the Crystallinity

To obtain a quantitative understanding of the reaction kinetics of the MO degradation, we applied a pseudo-first-order model, as expressed by the following equation, which is generally used for photocatalytic degradation processes if the initial concentration of pollutant is low:[25]

$\ln (C_o/C) = Kt$

where C_o and C are the concentrations of the dye in solution at times 0 and t, respectively, and K is the pseudo-first-order rate constant. Figure 7a depicts the photocatalytic re-

action kinetics of the MO degradation for the samples obtained at 240 °C based on the data plotted in Figure 4b. A rather good correlation to pseudo-first-order reaction kinetics ($R > 0.98$) was found from these results, with the reaction constant K increasing in the order Me-240 < Et-240 < Bu-240 < Pr-240 from 0.0104 to 0.0594 min^{-1} concomitantly with an increase in the crystallinity (increase in crystallite size and decrease in lattice strain), as can be seen in Figure 7b. A similar trend was also found for the samples obtained at 180 °C (see Supporting Information), with the same order of the photocatalytic reaction constant K (Me-180 < Et-180 < Bu-180 < Pr-180), which in this case ranges from 0.0095 to 0.0302 min^{-1}. Furthermore, the samples prepared at 240 °C are superior to the corresponding one(s) at 180 °C as regards both their crystallinity and their photocatalytic efficiency, which also confirms the dependence of the photocatalysis on the crystallinity.

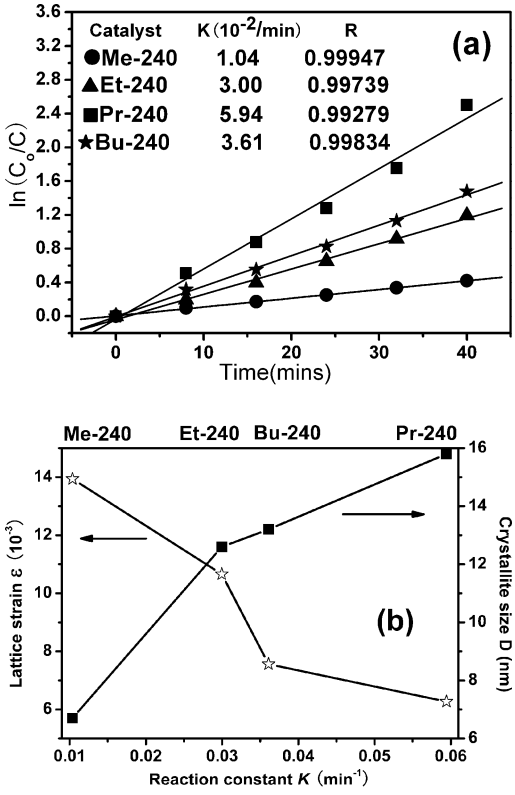

Figure 7. (a) Reaction kinetics of UV light induced MO degradation over samples synthesized at 240 °C; (b) effect of the crystallinity on the reaction constant K.

As mentioned above, the gradually increasing crystallinity should be mainly responsible for the photocatalytic improvements seen in the present system. Crystallinity has been shown to have a significant influence on the two most important processes during photocatalysis, namely charge-separation and charge-transport, as follows:[3a,26] (1) Highly crystallized anatase can promote charge-transfer from the particle's center to its surface. Residual strain in the poorly crystallized TiO_2 lattice leads to disorder and distortion of the TiO_2 matrix, which can have a severe scattering effect on charge-transport. Furthermore, an electron and a hole can migrate further in a crystal of larger crystallite size than in a smaller one, thereby allowing separation of the more reducing and oxidizing sites on the surface of the crystal. Volume recombination is therefore likely to occur less frequently. (2) It eliminates the crystal defects (impurities, dangling bonds, and microvoids) which can act as recombination centers for the electron/hole pairs, which means that surface recombination is greatly suppressed. It is therefore not surprising that Pr-240, with a crystallite size of about 14.8 nm and a lattice strain of about 7.27×10^{-3}, has the highest reaction constant for MO decomposition, which in this case is about six times that for Me-240.

Conclusions

Phase-pure anatase TiO_2 nanocrystals have been prepared by a facile solvothermal method in the absence of additives. The crystallinity can be controlled by using solvents with different dielectric constants. Thus, 2-propanol, which has a relatively low dielectric constant, results in a lower solubility of the solid metal oxide and a higher supersaturation degree in this system, which in turn leads to a greater number of nuclei, a sufficient supply of precursors, accelerated crystal growth, thereby promoting the crystallization of TiO_2 nanocrystals. Pr-240 has the highest crystallinity, in other words the largest crystallite size (14.8 nm) and lowest lattice strain (7.27×10^{-3}). This high crystallinity provides significantly improved charge transport and separation and eliminates crystal defects, thus contributing to the enhanced photocatalytic activity – the reaction constant K for MO decomposition by Pr-240 is almost six times that for Me-240. This paper has therefore shed some light on solvent selection for the designed synthesis of nano-TiO_2 with different crystallinity and the method reported herein has been shown to provide flexibility, selectivity, and efficiency for the designed synthesis of other functional nanomaterials.

Experimental Section

Synthesis: All chemicals were obtained commercially and used as received without further purification. Titanium *n*-butoxide [TNB, $Ti(OBu)_4$] was chosen as the precursor, and four different solvents, namely methanol, ethanol, 2-propanol, and *n*-butanol, were used as reaction media for the present solvothermal treatment. In a typical synthesis with ethanol as solvent, TNB (5.0 mL) was diluted in anhydrous ethanol (24.0 mL) and the mixture stirred for 10 min to obtain a pale-yellow solution. After dropwise addition of deionized water (1.0 mL) and stirring for 30 min, the homogeneous white sol was transferred into a Teflon-lined autoclave (50 mL capacity, 60% filling), which was heated to the desired temperature at a rate of 3 °C/min and maintained at this temperature without stirring for the proposed reaction time (6 h). The autoclave was then allowed to cool gradually to room temperature in air, and the as-prepared powders were collected by centrifugation (3000 r/min, 15 min), washed three times with anhydrous ethanol, and dried at 80 °C.

Characterization: The crystal structure and phase identification of the samples were carried out by Fast Fourier Transformation (FFT) and XRD (Rigaku DMax-2200) with a monochromatized Cu-$K_{\alpha 1}$ radiation source (λ = 0.15405 nm) at 1.6 kW (40 kV, 40 mA). Since peak broadening generally depends on lattice strain (ε) and crystallite size (D), these variables were determined separately by using the Williams and Hall equation [Equation (1)]:[17]

$$\beta\cos\theta = K\lambda/D + 2\varepsilon\sin\theta \quad (1)$$

where β is the full width at half maximum (FWHM) intensity observed, K the shape factor (assumed to be 0.90), and λ the wavelength of the Cu-$K_{\alpha 1}$ radiation (0.154056 nm). The FWHM of each diffraction line was determined from the profile measured at a scanning rate of 0.25°(2θ)/min^{-1}, which was calibrated by referring to a standard silicon powder for instrumental broadening. The plots of $\beta\cos\theta$ against $\sin\theta$ for different samples were approximated to be linear. D was calculated from the intercept of the extrapolation of this linear relation to the ordinate (i.e., $\sin\theta = 0$), and ε was determined from the slope of this linear relation. For poorly crystalline samples, the linear relationship between $\beta\cos\theta$ and $\sin\theta$ was not very clear. For highly crystalline samples, however, a good linearity was observed, and so reliable values of D and ε were obtained.[14] The band-gap energy (E_g) of the powders was determined from the UV/Vis diffuse reflectance spectrum obtained with a spectrophotometer (Hitachi U3010) equipped with an integrating sphere and with $BaSO_4$ as a reference in the wavelength range 250–800 nm. Field-emission TEM (JEM, 2100F) as well as HRTEM were used to study the morphology, crystallinity, and dimensions of the powders. The Brunauer–Emmett–Teller (BET) specific surface areas were determined from nitrogen sorption isotherms at 77 K with a Micromeritics ASAP2010 instrument and calculated from the linear part of the BET plot. Photocatalytic activity was determined as reported in our previous papers.[27] Methyl orange (MO) was used as a representative organic pollutant to evaluate the photocatalytic activity of as-prepared nano-TiO_2 under UV irradiation.

Supporting Information (see footnote on the first page of this article): Photocatalytic reaction kinetics of MO degradation over the samples obtained at 180 °C; TEM images for nano-TiO_2 obtained at 180 °C.

Acknowledgments

Financial support from the National 973 Program of China (grant no. 2007CB936704), the National Science Foundation of China (grant no. 50772123, and the Science and Technology Commission of Shanghai (grant no. 0752nm016) is gratefully acknowledged.

[1] S. Kim, B. Fisher, H. J. Eisler, M. Bawendi, *J. Am. Chem. Soc.* **2003**, *125*, 11466–11467.
[2] a) E. Aboelfetoh, R. Pietschnig, *Catal. Lett.* **2009**, *127*, 83–94; b) H. J. Yun, H. Lee, J. B. Joo, W. Kim, J. Yi, *J. Phys. Chem. C* **2009**, *113*, 3050–3055; c) D. S. Kim, S. Y. Kwak, *Appl. Catal. A* **2007**, *323*, 110–118; d) Z. Y. Xu, X. M. Chen, *Mater. Lett.* **1999**, *39*, 18–21; e) B. O'Regan, M. Gratzel, *Nature* **1991**, *353*, 737–740; f) E. Traversa, G. Gnappi, A. Montenero, G. Gusmano, *Sens. Actuators B* **1996**, *31*, 59–70; g) T. N. Smirnova, O. V. Sakhno, V. I. Bezrodnyj, J. Stumpe, *Appl. Phys. B* **2005**, *80*, 947–951; h) N. D. Abazovic, M. I. Comor, M. D. Dramicanin, D. J. Jovanovic, S. P. Ahrenkiel, J. M. Nedeljkovic, *J. Phys. Chem. B* **2006**, *110*, 25366–25370; i) A. Fujishima, K. Honda, *Nature* **1972**, *238*, 37–38.
[3] a) S. Bakardjieva, V. Stengl, J. Jirkovsky, N. Petrova, *J. Mater. Chem.* **2006**, *16*, 1709–1716; b) J. G. Yu, S. W. Liu, H. G. Yu, *J. Catal.* **2007**, *249*, 59–66; c) N. Venkatachalam, V. Murugesan, *J. Mol. Catal. A* **2007**, *273*, 177–185; d) J. G. Yu, G. H. Wang, B. Cheng, M. H. Zhou, *Appl. Catal. B* **2007**, *69*, 171–180.
[4] a) K. Suriye, P. Praserthdam, B. Jongsomjit, *Ind. Eng. Chem. Res.* **2005**, *44*, 6599–6604; b) K. M. Reddy, C. V. G. Reddy, S. V. Manorama, *J. Solid State Chem.* **2001**, *158*, 180–186.
[5] a) B. M. Wen, C. Y. Liu, Y. Liu, *New J. Chem.* **2005**, *29*, 969–971; b) J. H. Lee, Y. S. Yang, *Mater. Chem. Phys.* **2005**, *93*, 237–242; c) L. H. Kao, T. C. Hsu, H. Y. Lu, *J. Colloid Interface Sci.* **2007**, *316*, 160–167; d) H. H. Huang, *J. Nanosci. Nanotechnol.* **2008**, *8*, 2680–2683; e) S. J. G. Choi, K. Y. Park, *J. Nanopart. Res.* **2006**, *8*, 269–278.
[6] a) S. H. Lee, M. S. Kang, S. M. Cho, C. H. Chung, *J. Photochem. Photobiol. A: Chem.* **2001**, *146*, 121–128; b) C. S. Kim, B. K. Moon, S. T. Chung, S. M. Son, *J. Cryst. Growth* **2003**, *254*, 405–410; c) G. H. Li, K. A. Gray, *Chem. Mater.* **2007**, *19*, 1143–1146.
[7] a) J. Ovenstone, K. Yanagisawa, *Chem. Mater.* **1999**, *11*, 2770–2774; b) M. Gopal, W. J. M. Chan, L. C. DeJonghe, *J. Mater. Sci.* **1997**, *32*, 6001–6008.
[8] Y. Li, T. J. White, S. H. Lim, *J. Solid State Chem.* **2004**, *177*, 1372–1381.
[9] H. Kominami, M. Kohno, Y. Kera, *J. Mater. Chem.* **2000**, *10*, 1151–1156.
[10] a) C. C. Wang, J. Y. Ying, *Chem. Mater.* **1999**, *11*, 3113–3120; b) M. M. Wu, G. Lin, R. R. Xu, *Chem. Mater.* **2002**, *14*, 1974–1980; c) H. Cheng, J. Ma, L. Qi, *Chem. Mater.* **1995**, *7*, 663–671.
[11] X. F. Yang, H. F. Xu, M. M. Wu, *Eur. J. Inorg. Chem.* **2006**, 2229–2235.
[12] K. Byrappa, M. Yoshimura, *Handbook of Hydrothermal Technology*, William Andrew Publishing, New York, **2001**.
[13] J. P. Jolivet, *Metal Oxide Chemistry and Synthesis–From Solution to Solid State*, John Wiley & Sons, Chichester, **2003**.
[14] B. Tryba, M. Toyoda, A. W. Morawski, R. Nonaka, M. Inagaki, *Appl. Catal. B: Environ.* **2007**, *71*, 163–168.
[15] G. H. Tian, H. G. Fu, B. F. Xin, K. Pan, *J. Phys. Chem. C* **2008**, *112*, 3083–3089.
[16] R. J. Tayade, R. G. Kulkarni, R. V. Jasra, *Ind. Eng. Chem. Res.* **2006**, *45*, 922–927.
[17] G. K. Williamson, W. H. Hall, *Acta Metall.* **1953**, *1*, 22–31.
[18] M. Inagaki, R. Nonaka, B. Tryba, A. W. Morawski, *Chemosphere* **2006**, *64*, 437–445.
[19] a) J. W. Mullin, *Crystallization*, 3rd ed., Butterworth-Heinemann, Oxford, **1997**; b) A. D. Randolph, M. A. Larson, *Theory of Particulate Processes*, Academic Press, New York, **1988**.
[20] a) R. C. Xie, J. K. Shang, *J. Mater. Sci.* **2007**, *42*, 6583–6589; b) J. Zhang, L. D. Sun, C. H. Yan, *Chem. Mater.* **2002**, *14*, 4172–4177; c) J. S. Lee, S. C. Choi, *J. Eur. Ceram. Soc.* **2005**, *25*, 3307–3314; d) Z. L. Hua, X. M. Wang, J. L. Shi, *J. Eur. Ceram. Soc.* **2006**, *26*, 2257–2264.
[21] K. N. A. Sirachaya, M. Okorn, P. Piyasan, *Cryst. Growth Des.* **2006**, *11*, 2446–2450.
[22] a) T. Moeller, *Inorganic Chemistry*, Wiley, New York, **1952**; b) F. Franks, *Water – A Comprehensive Treatise*, Plenum Press, New York, **1973**.
[23] a) T. Adschiri, Y. Hakuta, K. Sue, K. Arai, *J. Nanoparticle Res.* **2001**, *3*, 227–235; b) C. H. Cho, M. H. Han, D. H. Kim, D. K. Kim, *Mater. Chem. Phys.* **2005**, *92*, 104–111; c) J. Li, H. C. Zeng, *J. Am. Chem. Soc.* **2007**, *129*, 15839–15847; d) H. G. Yang, H. C. Zeng, *J. Phys. Chem. B* **2004**, *108*, 3492–3495; e) H. Zhang, X. Y. Ma, D. R. Yang, *Chem. Commun.* **2008**, 5648–5650.
[24] Y. T. Moon, H. K. Park, I. S. Seog, *J. Am. Ceram. Soc.* **1995**, *78*, 2690–2694.

[25] J. M. Herrmann, H. Tahiri, Y. Ait-Ichou, G. Lassaletta, A. R. GonzalezElipe, A. Fernandez, *Appl. Catal. B* **1997**, *13*, 219–228.

[26] a) M. Toyoda, Y. Nanbu, M. Inagaki, *Appl. Catal. B* **2004**, *49*, 227–232; b) A. L. Linsebigler, G. Q. Lu, J. T. Yates, *Chem. Rev.* **1995**, *95*, 735–758; c) X. Chen, S. S. Mao, *Chem. Rev.* **2007**, *107*, 2891–2959; d) T. Peng, D. Zhao, K. Hirao, *J. Phys. Chem. B* **2005**, *109*, 4947–4952; e) B. Ohtani, Y. Ogawa, S. I. Nishimoto, *J. Phys. Chem. B* **1997**, *101*, 3746–3752.

[27] a) Z. C. Shan, J. J. Wu, F. F. Xu, F. Q. Huang, H. M. Ding, *J. Phys. Chem. C* **2008**, *112*, 15423–15428; b) X. P. Lin, F. Q. Huang, J. C. Xing, W. D. Wang, F. F. Xu, *Acta Mater.* **2008**, *12*, 2699–2705; c) X. P. Lin, T. Huang, F. Q. Huang, W. D. Wang, J. L. Shi, *J. Phys. Chem. B* **2006**, *110*, 24629–24634.

Received: March 2, 2009
Published Online: May 27, 2009

